Quasi-Two-Dimensional Melting in Porous Media: Effect of Multi-layers and Cross-Over in Scaling Behavior

Malgorzata Sliwinska-Bartkowiak[1], Ravi Radhakrishnan[2] and Keith E Gubbins[3]

[1] *Instytut Fizyki, Uniwersytet im Adama Mickiewicza, Poznan, Poland*

[2] *Department of Bioengineering, University of Pennsylvania, Philadelphia, PA, USA*

[3] *Department of Chemical Engineering, North Carolina State University, Raleigh NC, USA.*

(January 4, 2005)

Abstract

We report molecular simulation and experimental results for simple fluids adsorbed in activated carbon fibers (ACF), where the adsorbed phase consists of either one or two molecular layers. Our molecular simulations involve smooth pore-walls for large system sizes and a systematic system size-scaling analysis. We provide calculations of the Ginzburg parameter to monitor the self-consistency of our finite size simulation results, based on which we establish that for system sizes smaller than 60 molecular diameters, fluctuations are too large to uphold the finite size simulation results. We present scaling analysis and free energy results for a system size of 180 molecular diameters. Our scaling analysis reveals a two-stage melting in our bilayer system consistent with KTHNY scaling for the order parameter correlation functions. Based on the Lee-Kosterlitz scaling of the free energy surface, we establish that the transitions are first order in the thermodynamic limit. Similar results for a monolayer established that the transitions were continuous. We provide scaling arguments to suggest that the change in the order of the transitions in going from a monolayer to bilayer adsorbed system results from the interactions of defects in the multilayers. We also report experimental measurements

of CCl_4 and aniline (with two confined molecular layers) adsorbed in ACF. The differential scanning calorimetry and dielectric relaxation spectroscopy measurements for the transition temperatures are in quantitative agreement with each other and with our simulation results. We also report nonlinear dielectric effect (NDE) measurements and show that our data is consistent with the NDE scaling law for the KTHNY scenario, which we derive. Finally, we discuss the significance of the six-fold corrugated potential and the effect of the strength of pore-wall potential on the melting behavior. Both the simulations and experiments show that the hexatic phase is stabilized by confinement in carbon pores; for carbon tetrachloride and aniline the hexatic phase is stable over a temperature range of 55 K and 26 K, respectively. Moreover, this stability increases as the ratio of fluid-wall to fluid-fluid attraction increases.

I. INTRODUCTION

For continuous symmetry breaking transitions (such as melting transitions) in two-dimensions, the Mermin-Wagner theorem states that true long range order ceases to exist[1]. Halperin and Nelson proposed the "KTHNY" (Kosterlitz-Thouless-Halperin-Nelson-Young) mechanism for melting of a crystal in two dimensions[2], which involves two transitions of the Kosterlitz-Thouless (KT) kind[3]. The crystal to hexatic transition occurs through the unbinding of dislocation pairs, and the hexatic to liquid transition involves the unbinding of disclination pairs. Each KT transition is accompanied by a non-universal peak in the specific heat above the transition temperature, associated with the entropy liberated by the unbinding of the vortex (dislocation or disclination) pairs, and by the disappearance of the stiffness coefficient associated with the presence of quasi-long-range order in the system. The KTHNY theory predicts that the correlation function associated with the translational order parameter in the crystal decays algebraically with exponent $\eta < 1/3$, while long range orientational order is maintained, and the correlation function associated with the orientational order parameter in the hexatic phase decays algebraically with exponent $0 < \eta_6 < 1/4$ while there is no translational order. The KTHNY theory is an analysis of the limit of stability of a two-dimensional solid, since it neglects the existence of the liquid phase and thereby does not impose an equality of the chemical potentials of the solid and liquid phases as the criterion for melting. Therefore, other pathways for two-dimensional melting can not be ruled out. For example, it is possible for the dislocation unbinding transition to be pre-empted by grain-boundary-induced melting, as shown by the work of Chui[4], which predicts that the critical value of the defect core energy (E_c) above which the melting cross-over from grain boundary induced melting to two-stage KTHNY melting is $E_c = 2.8 k_B T^5$. Excellent reviews are available on the subject of two-dimensional melting[5] (also see section II).

In this paper we report molecular simulation and experimental results for simple fluids adsorbed in activated carbon fibers (ACF), whose pore widths are such that they can accommodate one or two molecular layers. Our computer simulations involve smooth walls for

large system sizes, and we perform a systematic scaling analysis. We provide calculations of the Ginzburg parameter to monitor the self-consistency of our finite size simulation results for system sizes (box lengths) up to 180 molecular diameters. We also present scaling analysis and free energy results for a system size of 180 molecular diameters. Based on the Lee-Kosterlitz scaling of the free energy surface, we establish the nature (first order vs. continuous) of the transitions. We also report experimental measurements based on differential scanning calorimetry, dielectric relaxation spectroscopy, and nonlinear dielectric effect for CCl_4 and aniline (with two confined molecular layers) adsorbed in ACF.

II. PREVIOUS WORK

Experimental and computer simulation studies on the subject of two-dimensional melting often have the underlying objective of establishing whether or not the pathway of melting conforms to KTHNY behavior: (1) Does melting occur in two stages mediated by a hexatic phase? (2) Do the order parameter correlation functions associated with the crystal and hexatic phases have the appropriate scaling behavior? (3) Are the observed phase transitions first order or second order in the thermodynamic limit? The different experimental systems explored in this regard include *free-standing liquid-crystalline (LC) films*[6,7], *confined colloidal suspensions*[8–11], and *adsorbed fluid on a planar substrate*[12–19].

Computer Simulation Studies of Two-Dimensional Melting. Early simulation studies on small ($\lesssim 10000$ atoms), strictly two-dimensional systems failed to provide compelling evidence to support the KTHNY melting scenario[5,20–22]. For systems with repulsive interactions, it was shown by Bagchi et. al.[23], using a systematic scaling analysis on large system sizes ($\simeq 64,000$ atoms), and subsequently by Jaster[24], that the equilibrium properties are indeed consistent with the KTHNY theory of melting (a single stage melting via first-order transitions with finite correlations was ruled out). Bagchi et. al.[23] have also observed a first order single stage melting for a two-dimensional system of disks interacting with a soft

repulsive potential for a *small system size*, crossing over to *two-stage continuous* melting consistent with KTHNY scaling for larger system sizes, suggesting the earlier studies were plagued by serious system size effects.

Computer simulation studies that directly mimic the liquid-crystalline thin film experiments have not been attempted owing to the complexity of the molecular architecture and experimental conditions. Idealized simulations of spheres confined between hard walls and interacting with each other via a model potential that mimic the screened potential in colloidal systems[9] (but otherwise neglect the solvent) have been performed by Bladon and Frenkel[25], and Zangi and Rice[26]. The former study reported a strong dependence (and qualitatively different phase diagrams of the melting region) of melting behavior on the parameters of the inter-molecular interaction of a two-dimensional square-well fluid, and attributed the difference to the changing values of the defect core energy[25]; in particular, the study puts the two-dimensional hard disks in the single-stage first order melting regime (rather than the KTHNY regime). In subsequent experiments and simulations carried out by Rice and co-workers using two different screened (effective) potentials with which confined colloidal spheres interact[9,10,26], a strong dependence of the melting scenario on the inter-particle interaction, consistent with the computer simulation study by Bladon and Frenkel[25] was reported. A clear picture regarding the differing scenarios has not yet emerged due to: (a) the experimental studies on colloidal systems are faced with the question of attainment of thermodynamic equilibrium[9,10], while the simulation results are for a small system size[25], and are therefore subject to finite-size effects; (b) the calculated value for the defect core energy E_c for hard disks lie in the KTHNY regime[27]; (c) the qualitative behavior of these studies in the limit of a hard sphere potential differs from that of a recent simulation study by Jaster[24] on a large 2-d system of hard disks.

Several computer simulations aimed to mimic an adsorbed fluid on graphite have been reported[28–30]. Abraham[28] has reported several studies of xenon on graphite in which the melting transition temperatures are in quantitative agreement with experiment. However, the existence of an intrinsic hexatic phase could not be demonstrated by the simulations,

which were performed on fairly small system sizes. Similar conclusions were drawn by Roth[29] based on simulations of krypton on graphite, again for a small system size. Alavi[30] reported a simulation study of CD_4 on MgO (using a small system size) with melting behavior consistent with the KTHNY scenario and a defect core energy of $9k_BT$ (KTHNY regime). One notable difference between the CD_4 on MgO system and the Kr, Xe on graphite systems is that, in the former case, due to the molecular structure of CD_4 adsorbed on MgO, the relevant degrees of freedom at the temperature of study make the adsorbate move in a field-free manner.

In summary, the simulations on small systems have failed to provide compelling evidence of the melting picture, and therefore can not be used conclusively to fill in the gaps or interpret experimental measurements. While the system-size scaling analysis for large system sizes in the simulations of Bagchi et. al.[23] (which indicated a KTHNY melting scenario) clearly underlines the need to use large system sizes in studying the two-dimensional melting problem, even such methods do not provide a source of distinction between the first-order and continuous nature of the transition.

Two-dimensional Melting in Adsorbates Confined in Porous Media. Activated carbon fibers (ACF) possess micro-crystallites made up of graphene sheets that tend to align in similar directions, with slit shaped voids between the microcrystals. The spontaneous ordering of the molecules adsorbed in these voids into distinct two- dimensional molecular layers (analogous to the structure of a smectic-A phase in liquid crystals) makes the adsorbed phase a quasi-two-dimensional system. Microporous ACF can be prepared having a range of mean pore sizes, ranging from those that can accommodate just a single layer of the adsorbate in the micropores to those that can accommodate a few layers[31]. The microcrystals in ACF are themselves arranged as an amorphous matrix; therefore the maximum in-plane correlation length of the adsorbed fluid is thought to be limited by the average size of the microcrystals. Real samples of ACF have different average sizes for their microcystals (ranging from 5 nm to 100 nm) depending on the method of activation and the source of the carbon material

used to derive the porous material[31]. Electron micrographs are commonly employed to determine the average size of the microcrystals, while nitrogen adsorption isotherms are used to determine the average pore size and pore size distribution. The substrate field induced by the porous matrix is thought to have a six-fold symmetry like that of graphite. Additionally, due to the high density of carbon atoms in the graphene microcrystals, the confined fluid feels a large potential well, and this increases in depth for decreasing pore sizes; this unique feature induces pronounced layering effects even in multi-layer adsorbate phases, each layer effectively being two-dimensional. The quasi-two-dimensional phase of adsorbed simple fluids (spherical molecules) do not have the complication of additional coupling due to any herring bone symmetry, in contrast to the LC systems. In addition, owing to the nanoscopic length scales, these systems are thermally driven and can be studied under equilibrium (a challenging issue for the colloidal systems). The large value of the defect core energy[30] in adsorbed systems and the role of out-of-plane motions in stabilizing the hexatic phase in these quasi-two-dimensional systems have been noted earlier[5,26].

III. MOLECULAR SIMULATION METHODS

We performed Grand Canonical Monte Carlo (GCMC) simulations of a fluid adsorbed in slit-shaped pores of width H, where H is defined as the perpendicular distance between the planes passing through the nuclei of the first layer of molecules that make up the pore walls of the slit-shaped pore. The interaction between the adsorbed fluid molecules is modeled using the Lennard-Jones (12,6) potential with size and energy parameters, $\sigma_{\rm ff}$, and $\epsilon_{\rm ff}$. The Lennard -Jones potential was cut-off at a distance of $5\sigma_{\rm ff}$, beyond which it was assumed to be zero. The pore walls were modeled as a continuum of LJ molecules using the"10-4-3" Steele potential[32], given by,

$$\phi_{\rm fw}(z) = 2\pi\rho_{\rm w}\epsilon_{\rm fw}\sigma_{\rm fw}^2\Delta\left[\frac{2}{5}\left(\frac{\sigma_{\rm fw}}{z}\right)^{10} - \left(\frac{\sigma_{\rm fw}}{z}\right)^{4} - \left(\frac{\sigma_{\rm fw}^4}{3\Delta(z+0.61\Delta)^3}\right)\right] \qquad (1)$$

Here, the σ's and ϵ's are the size and energy parameters in the Lennard-Jones (LJ) potential, the subscripts f and w denote fluid and wall respectively, Δ is the distance between two

successive lattice planes of pore wall, z is the coordinate perpendicular to the pore walls and $\rho_{\rm w}$ is the number density of the wall atoms. For a given pore width, H, the total potential energy from both walls is given by,

$$\phi_{\rm pore}(z) = \phi_{\rm fw}(z) + \phi_{\rm fw}(H - z) \tag{2}$$

The strength of attraction of the pore walls relative to the fluid-fluid interaction is determined by the coefficient α,

$$\alpha = \frac{\rho_{\rm w}\epsilon_{\rm fw}\sigma_{\rm fw}^2\Delta}{\epsilon_{\rm ff}} \tag{3}$$

in equation 1. The fluid-fluid interaction parameters were chosen to be those for CCl_4[33], with $\sigma_{\rm ff} = 0.514$ nm, $\epsilon_{\rm ff}/k_B = 395$ K; with these parameters the freezing temperature of bulk CCl_4 is reproduced. The parameters for the graphite pore wall interaction to mimic the micropores in ACF were taken from Steele[32], ($\sigma_{\rm ww} = 0.34$ nm, $\rho_{\rm w} = 114$ nm^{-3}, $\epsilon_{\rm ww}/k_B = 28$ K, and $\Delta = 0.335$ nm). The Lorentz-Berthlot mixing rules, together with the ff and ww parameters, were used to determine the values of $\sigma_{\rm fw}$ and $\epsilon_{\rm fw}$. The simulation runs were performed by fixing the chemical potential, μ, the volume ,V, of the pore and the temperature, T. Two pore-widths $H = 1\sigma_{ff}+\sigma_{fw} = 0.91$ nm (monolayer of adsorbate) and $H = 2\sigma_{ff}+\sigma_{fw} = 1.41$ nm (bilayer of adsorbate) , were chosen for study. The rectilinear dimension of the cells were therefore $180\sigma_{\rm ff} \times 180\sigma_{\rm ff} \times H$ (93 nm $\times$ 93 nm $\times$ H nm). Typically the system consisted of up to 64,000 adsorbed fluid molecules. Periodic boundary conditions were employed in the x and y directions (the xy-plane being parallel to the pore walls) and no long range corrections were applied. The adsorbed molecules formed distinct molecular layers parallel to the plane of the pore walls. The simulation was set up such that insertion, deletion and displacement moves were chosen at random with equal probability. The calculations for the larger of the chosen pore-width also enable a direct comparison to be made with experimental measurements for CCl_4 confined in porous pitched-based activated carbon fiber ACF A-10, of mean pore width $H = 1.4$ nm. We expect the approximation of a structureless graphite wall to be a good one here, since the diameter of the LJ molecule (0.514 nm) is much larger than the C-C bond length in graphite (0.14 nm). The state conditions were such that the

confined phase was in equilibrium with bulk LJ CCl_4 at 1 atm. pressure. The simulations were started from a well equilibrated confined liquid phase at $T = 400$ K, and in successive simulation runs the temperature was reduced. Equilibration was for a minimum of 11 billion steps; the standard deviation of block averages of total energy of the system was 10^{-4} and the rate of insertion was equal to that of deletion to a factor of 10^{-6}.

Free Energy Determination. Motivated by the work of Frenkel and co-workers[34–36], we employ the Landau free energy approach that was successful in our earlier studies[33,35–37]. The Landau-Ginzburg formalism[38] involves choosing a spatially varying order parameter $\Phi(\vec{r})$, that is sensitive to the degree of order in the system. We use a two- dimensional bond orientational order parameter to characterize the orientational order in each of the molecular layers that is defined as follows[39]:

$$\Psi_{6,j}(\vec{\rho}\,) \;=\; \frac{1}{N_b}\sum_{k=1}^{N_b} \exp(i6\theta_k), \tag{4}$$

where N_b is the number of nearest-neighbor bonds and θ_k is the bond angle (see below); the summation is over the (imaginary) bonds joining the central molecule to its nearest neighbors. $\Psi_{6,j}(\vec{\rho}\,)$ measures the hexagonal bond order at position $\vec{\rho}$ in the xy plane within each layer j, and is calculated as follows. Nearest neighbors were identified as those particles that were less than a cutoff distance $r_{\rm nn}$ away from a given particle, and belonged to the same layer. We used a cutoff distance $r_{nn} = 1.3\ \sigma_{\rm ff}$, corresponding to the first minimum of $g(r)$. The orientation of the nearest neighbor bond is measured by the θ coordinate, which is the angle that the projection of the nearest-neighbor vector on to the xy-plane makes with the x axis. $\Psi_{6,j}(\vec{\rho}\,)$, is calculated using equation 4, where the index k runs over the total number of nearest neighbor bonds N_b at position $\vec{\rho}\,$, in layer j. The order parameter $\overline{\Psi}_{6,j}$ in layer j is given by $\overline{\Psi}_{6,j} \;=\; |\int d\vec{\rho}\,\Psi_{6,j}(\vec{\rho}\,)| \,/\, \int d\vec{\rho}$. For the case of LJ CCl_4 in slit-shaped pores, where there is significant ordering into distinct molecular layers, the spatially varying

order parameter $\Phi(\vec{r}\,)$ can be reduced to $\Phi(z)$, and can be represented by,

$$\Phi(z) \;=\; \sum_{j=1}^{n} \overline{\Psi}_{6,j}\, \delta(z - \hat{z}_j) \tag{5}$$

In equation (5), the sum is over the number of adsorbed molecular layers, and $\hat{z}_j$ is the z coordinate of the plane in which the coordinates of the center of mass of the adsorbed molecules in layer j are most likely to lie. It must be recognized that each of the $\overline{\Psi}_{6,j}$'s are variables that can take values in the range $[0, 1]$; the number of layers is $n = 1$ or $n = 2$ in our system. The histograms are collected to evaluate the probability distribution $P[\overline{\Psi}_{6,1}, \overline{\Psi}_{6,2}]$.

The Landau free energy[38] $\Lambda[\overline{\Psi}_{6,1}, \overline{\Psi}_{6,2}]$ (for the bilayer system) is given by,

$$\Lambda[\overline{\Psi}_{6,1}, \overline{\Psi}_{6,2}] \;=\; -k_B T\, \ln(P[\overline{\Psi}_{6,1}, \overline{\Psi}_{6,2}]) \;+\; \text{Constant} \tag{6}$$

The Landau free energy is computed by a histogram method combined with umbrella sampling[40], using the probability distribution $P[\overline{\Psi}_{6,1}, \overline{\Psi}_{6,2}]$. Detailed procedures to collect statistics, construct the histograms and to choose the the weighting functions for performing the umbrella sampling are described elsewhere[34–36]. The grand free energy of a particular phase A, $\Omega_A = -k_B T\, \ln(\Xi)$ (where Ξ is the partition function in the grand canonical ensemble), is related to the Landau free energy by,

$$\exp(-\beta\Omega) \;=\; \prod_{j=1}^{2} \int_j d\overline{\Psi}_{6,j}\, \exp(-\beta\Lambda[\overline{\Psi}_{6,1}, \overline{\Psi}_{6,2}]) \tag{7}$$

where the limits of integration in equation 7 are from the minimum value of $(\overline{\Psi}_{6,1}, \overline{\Psi}_{6,2})$ to the maximum value of $(\overline{\Psi}_{6,1}, \overline{\Psi}_{6,2})$ that characterize the phase A. The grand free energy is computed via numerical integration of equation 7. The two- dimensional, in-plane positional and orientational correlation functions ($g_j(r)$ and $G_{6,j}(r)$ of layer j), were monitored to keep track of the nature of the confined phase. The positional pair correlation function is the familiar radial distribution function. The orientational pair correlation function is $G_{6,j}(\rho) = \langle \Psi^*_{6,j}(0)\Psi_{6,j}(\rho)\rangle$, where $\vec{\rho} = x\hat{e}_x + y\hat{e}_y$. The above equations correspond to the two-layer case. For the one layer case, the Landau free energy reduces to $\Lambda[\overline{\Psi}_{6,1}]$ and the index j in equation 7 assumes a value of 1.

IV. EXPERIMENTAL METHODS

Sample Preparation. The liquid samples were reagent grade chemicals, and were distilled twice prior to use in the experiment. The conductivities of the purified dipolar fluid samples were found to be less than 10^{-10} ohm^{-1}m^{-1}. The microporous activated carbon fiber (ACF) samples used were commercially available from Osaka gas company, Japan, with a pore size distribution of about 5% around the mean pore diameter[41]. ACF samples with an average pore width of 1.41 nm were used. The pore samples were previously characterized by Oshida and Endo by obtaining electron micrographs[31,42], and by Kaneko and co-workers using nitrogen adsorption measurements[41]. The characterization results for ACF showed that these amorphous materials consisted of uniform pores formed by graphitic microcrystals, with an average microcrystal size of 7–10 nm[31].

Differential Scanning Calorimetry (DSC). A Perkin-Elmer DSC7 differential scanning calorimeter was used to determine the melting temperatures and latent heats of fusion, by measuring the heat released in the melting of aniline and CCl_4. The temperature scale of the DSC machine was calibrated using the melting temperature of pure fluid from the literature. The temperature scanning rates used for the melting and freezing runs varied from 0.1K/min to 0.5K/min. The background of each raw DSC spectrum was subtracted, based on a second-order polynomial fit to the measured heat flow away from the signals of interest. The melting temperatures in the bulk and confined systems were determined from the position of the peaks of the heat flow signals, and the latent heats were determined based on the scaled area under these signals. The melting temperature was reproducible to within 0.5 $^{\mathrm{O}}$C for fluid adsorbed in pores. The latent heats were reproducible to within 5%.

Dielectric Relaxation Spectroscopy (DRS). The relative permittivity of a medium, $\kappa^* = \kappa_r - i\kappa_i$, is in general a complex quantity whose real part κ_r (also known as the dielectric constant) is associated with the increase in capacitance due to the introduction of

the dielectric. The imaginary component κ_i is associated with mechanisms that contribute to energy dissipation in the system, due to viscous damping of the rotational motion of the dipolar molecules in alternating fields. The latter effect is frequency dependent. The experimental setup consisted of a parallel plate capacitor of empty capacitance $C_o = 4.2$ pF. The capacitance, C, and the tangent loss, $\tan(\delta)$, of the capacitor filled with the fluid between the plates were measured using a Solartron 1260 gain impedance analyzer, in the frequency range 1 Hz - 10 MHz, for various temperatures. For the case of the adsorbate in ACF, the sample was introduced between the capacitor plates as a suspension of ground ACF particles of 0.1 mm mesh ACF particles in pure fluid. Due to the large conductivity of ACF, the electrodes were blocked by teflon. The relative permittivity is related to the measured quantities by:

$$\kappa_r \;=\; \frac{C}{C_o};\; \kappa_i \;=\; \frac{\tan(\delta)}{\kappa_r} \tag{8}$$

In equation (8), C is the capacitance, C_o is the capacitance without the dielectric and δ is the angle by which current leads the voltage. The complex dielectric permittivity, $\kappa^* = \kappa_r - i\kappa_i$, is measured as a function of temperature and frequency.

For an isolated dipole rotating under an oscillating electric field in a viscous medium, the Debye dispersion relation is derived using classical mechanics[43],

$$\kappa^* \;=\; \kappa_{\infty,r} \;+\; \frac{\kappa_{s,r} - \kappa_{\infty,r}}{1 + i\omega\tau} \tag{9}$$

Here ω is the frequency of the applied potential and τ is the orientational (rotational) relaxation time of a dipolar molecule. The subscript s refers to static permittivity (low frequency limit, when the dipoles have sufficient time to be in phase with the applied field). The subscript ∞ refers to the optical permittivity (high frequency limit) and is a measure of the induced component of the permittivity. Further details of the experimental methods are described elsewhere[44,45]. The dielectric relaxation time (molecular orientational relaxation time for dipolar molecules) was calculated by fitting the dispersion spectrum of the complex permittivity near resonance to the Debye model of orientational relaxation.

Nonlinear Dielectric Effect (NDE). The nonlinear dielectric effect (NDE) is defined as the permittivity change, $\Delta\epsilon$, of the medium in a strong electric field, E:

$$\mathrm{NDE} = \frac{\Delta\epsilon}{\mathrm{E}^2} = \frac{\epsilon_{\mathrm{E}} - \epsilon_{\mathrm{E}=0}}{\mathrm{E}^2} \tag{10}$$

where ϵ_E is the permittivity of the medium in a field E. The permittivity ϵ is related to the dielectric constant κ_r by the relationship $\kappa_r = \epsilon/\epsilon_o$, ϵ_o being the permittivity in vacuum. Note that within linear response (for weak fields), the permittivity is independent of the applied electric field; However, for strong fields, the most general form for the permittivity (consistent with field reversal invariance) can be written as $\epsilon_E = \epsilon_{E=0} + bE^2 + cE^4 + \cdots$. By definition, NDE in equation 10 represents the first order (non-linear) response consistent with the general equation. The NDE was measured using the pulse method using rectangular millisecond pulses of the electric field with amplitudes ranging from 4×10^7 to 9×10^7V/m. The separation between the invar electrodes in the measuring condenser was 2×10^{-4}m, and the changes in the capacitance were measured to an accuracy of 5×10^{-4}pF[46].

V. MOLECULAR SIMULATION RESULTS

Our simulations were made to mimic two experimental systems of CCl_4 confined in ACF with one as well as two confined molecular layers. The orientational correlation function $G_{6,j}(r)$ for equilibrated liquid, hexatic and crystal phases are shown in figure 1 . The long- Fig. 1
range orientational order in the crystal phase, the algebraic decay of orientational order in the hexatic phase and the exponential decay of orientational order in the liquid phase are captured in the plots. Since the phases are characterized by long-ranged correlations, we check for the attainment of equilibrium and artifacts due to finite size of the simulations as described below.

Simulation results are always for a finite system size, and system-size effects can not be avoided. When the state conditions are such that the relevant order-parameter correlation length ξ approaches or exceeds the spatial extent of the simulation cell L, the system crosses

over to a mean-field behavior[47,48]. For correlations in the bond-orientational order parameter, this is the case in the hexatic phase at all temperatures, and in the liquid phase near the liquid-hexatic transition. Under these circumstances, the self consistency of the mean field result is checked by calculating the Ginzburg parameter $\gamma_{\rm GL}$[49],

$$\gamma_{\rm GL} \;=\; \frac{\langle \overline{\Psi}_{6,j}^{2} \rangle}{\langle \overline{\Psi}_{6,j} \rangle^{2}} \;=\; \frac{I(L)}{\langle \overline{\Psi}_{6,j} \rangle^{2}} \;-\; 1. \tag{11}$$

where $L^2 \times H = V$, the volume of the system, L is the length of the simulation box, and $I(L)$ is given by

$$I(L) = \frac{\int_V \, d\vec{\rho}\, G_{6,j}(\rho)}{\int_V \, d\vec{\rho}} \tag{12}$$

The Ginzburg parameter gives the ratio of the variance in the order parameter (due to thermal fluctuations) to the square of the average value of the order parameter. Mean field results are clearly suspect in the regime $\gamma_{\rm GL} \gtrsim 1$, when long-range fluctuations are likely to destroy the observed order in the finite size simulations. If $\gamma_{\rm GL} \ll 1$, the simulations are self-consistent, and the ordered phase observed in the simulations is stable against thermal fluctuations. The Ginzburg parameter for different system sizes is calculated (using equation 11) by numerically integrating equation 12, and are reported in Table I. Our calculations for the bilayer system ($H = 1.41$ nm) indicate that the simulation results for these quasi-two-dimensional systems are only reliable for systems sizes $\gtrsim 60\sigma_{\rm ff}$. For smaller system sizes, the bond-orientational order parameter fluctuations are too large to validate the finite size results from computer simulations. Therefore, we report the free energy calculations and scaling behavior for system sizes of 60 and $180\sigma_{\rm ff}$.

Tab I

To quantify the scaling properties of the orientational correlation function (figure 1) in each phase, we plot $\log[I(L_B)/I(L)]$ as a function of $\log[L_B/L]$ in figure 2, for different values of the block length. The block length $L_B < L$ defines the subsystem $L_B \times L_B \times H$ for which the integrals (equation 12) were evaluated; the integrals $I(L_B)$ and I_L were calculated by numerically integrating equation 12. The expected KTHNY scaling for liquid, hexatic,

Fig. 2

and crystal are given by[2]:

$$G_{6,j}(r) \sim \begin{cases} \exp(-r/\xi) & \text{liquid} \\ r^{-\eta} & \text{hexatic} \\ \text{Constant} \neq 0 & \text{crystal} \end{cases} \tag{13}$$

where ξ is the correlation length and η is the exponent characterizing the algebraic decay of the order parameter correlation function. (The exponent η has its origins from the Ornstein-Zernikie formalism[50] discussed later, however, the exponent values and functional forms for liquid-liquid critical phenomena and KTHNY formalisms are different from one-another). Equations 12 & 13 lead to the following scaling for $I(L)$:

$$I(L) = \begin{cases} \text{Constant}/L^2 & \text{liquid} \\ L^{-\eta}/(2-\eta) & \text{hexatic} \\ \text{Constant} \neq 0 & \text{crystal} \end{cases} \tag{14}$$

Therefore, in figure 2, a slope of -2 corresponds to the liquid phase having a finite correlation length; a slope of $-1/4$ corresponds to an algebraic decay of $G_{6,j}(r)$ with exponent $-1/4$ and is observed for the hexatic phase near the hexatic-crystal transition; a slope of 0 is observed for the crystal phase, confirming the true long-range orientational order. The scaling properties shown in figure 2 is further evidence for the attainment of equilibrium in our simulations.

The order of the phase transition was determined by examining the dependence of the free energy barrier separating two phases as a function of system size. In doing so, we consider only those system sizes for which $\gamma_{\mathrm{GL}} \ll 1$. In order to determine the order of the phase transition using the Lee-Kosterlitz scaling analysis[51] of the free energy surface, we obtained the Landau free energy functions at the exact transition temperatures for the corresponding system size. This was done as follows: the Landau free energy surface was calculated at a temperature close to the transition, from which we calculated the grand free energies at that temperature. Then, by numerically integrating the Clausius-Claperon

equation, $d(\Omega/T)/d(1/T) = \langle U \rangle - \mu\langle N \rangle$, we located the exact transition temperature. The Landau free energy function was re-calculated at the transition temperature by using a weighting function equal to $\exp(\beta\Lambda[\overline{\Psi}_{6,j}])$ from the initial calculation. This procedure was repeated for each system size. The Landau free energy and the grand free energy results for the system size of $180\sigma_{\rm ff}$ are provided in figure 3. The relative stability of the liquid, hexatic and crystalline phases are inferred from the Landau free energy plot (figure 3), and the exact transition temperatures are given by the grand free energy plot (figure 4). For the bilayer adsorbed fluid, the free energy barrier separating hexatic and crystal phases is a linear function of system size (figure 3a). This implies that the mechanism of phase transition is via nucleation and is a clear indication of a first order phase transition in the thermodynamic limit. The critical nucleus at the transition temperature is equal to the system size, implying a L^{d-1} (d being the dimensionality of the system) dependence on system size[51]. In contrast to the bilayer case, the Lee-Kosterlitz scaling of the free energy surface for the adsorbed monolayer ($H = 0.91$ nm) in figure 3b establishes that the transitions are continuous in the monolayer. In this case the free energy barrier separating the liquid and the hexatic phase is independent of system size, a clear signature of second order transition[51]. We attribute this remarkable change in the mechanism of phase transition (spinodal decomposition in the monolayer to nucleation in the bilayer) to the interaction of defect structures across layers (see section VII).

Fig. 3

Fig. 4

VI. EXPERIMENTAL RESULTS

The DSC and DRS results for CCl_4 and aniline confined in ACF are provided in figures 5 and 6. The DSC scans show two peaks for each fluid reminiscent of liquid-hexatic (high temperature) and hexatic-crystal (low temperature) heat capacity peaks associated with Kosterlitz-Thouless phase transitions. The DRS measurements for the dielectric constant for confined aniline confirm the existence of two phase transitions (figure 6a). In addition, the molecular orientational relaxation times τ, (figure 6b) are consistent with the

Figs. 5,6

existence of liquid (τ ∼ns), hexatic ($\tau \sim \mu$s), and crystalline (τ ∼ms) phases. The transition temperatures from simulations and DSC for CCl_4 are in good agreement; also, the transition temperatures inferred from the DSC and DRS results for aniline are in agreement (Table II).

The NDE measurements for confined CCl_4 and aniline in ACF are provided in figure 7 and Table II. The NDE signals show signatures of divergence at the liquid-hexatic and hexatic-crystal transition temperatures. The NDE results for the transition temperatures for CCl_4 and aniline are in near quantitative agreement with the simulation result, and also with those from DSC, and DRS (Table II). Below, we show that the scaling of the NDE signal with temperature is consistent with the KTHNY theory for liquid-hexatic and hexatic-crystal transitions.

Fig. 7

Tab II

It was empirically known that the dipolar fluctuations associated with polarizability contributed to a positive signal for NDE. The anomalous increase in NDE in the vicinity of the phase transition point, reflecting the onset of long-range correlations and associated dipolar fluctuations in the system, has been experimentally documented[45]. Based on a droplet model for treating critical fluctuations by Oxtoby and Metiu[53], the dipolar fluctuations near a critical point have been correlated (linearly) with the relevant order parameter fluctuations. De Gennes[54] showed that the conformity to the droplet model by Oxtoby and Metiu[53] immediately leads to NDE scaling laws that are similar to those for critical fluctuations in light scattering experiments. The scaling law for critical opalescence in light scattering (where the order parameter correlation function is $g(r)$ associated with density fluctuations) is given by the familiar expression[49],

$$I(\vec{q}) = \langle \sum_{\alpha,\beta=1}^{N} \exp(i\vec{q}\cdot\vec{x}_\alpha)\, \exp(i\vec{q}\cdot\vec{x}_\beta)\rangle \;=\; N\left[1 \;+\; \int g(r)\, \exp(i\vec{q}\cdot\vec{r})\, d^d r.\right] \qquad (15)$$

In the above equation, $I(\vec{q}) = NS(\vec{q})$, is the intensity measured in scattering experiments, $S(\vec{q})$ is the familiar structure factor, d is the number of dimensions and N the total number of molecules. The double summation is over the total number of molecules, where $\vec{x}_\alpha, \vec{x}_\beta$ represent the coordinate vector of the given molecule. The second equality in equation 15 follows from evaluating the ensemble average[49]. By employing the extended Ornstein-Zernikie

representation[50] for the density-density correlations (above T_c), namely,

$$g(r) - 1 \sim \frac{1}{r^{d-2+\eta}} \exp(-r/\xi), \tag{16}$$

where ξ is the correlation length. The integral in equation 15 in the limit $q \to 0$ reduces to

$$I(q) \sim \xi^{d-1-\eta}. \tag{17}$$

The equation 16 corresponds to Fischer's extension of the original Ornstein-Zernikie formalism to alleviate a logarithimic divergence of $g(r)$ for large r in two-dimensions. Therefore, the equation provides the definition for the critical exponent η. The exponent satisfies the equality $(2-\eta)\nu = \gamma$, for systems with Ising symmetry, where ν (defined below) is the critical exponent associated with the correlation length, and γ that with isothermal compressibility.

According to the droplet model[53], the analogous expression for NDE is given by,

$$\text{NDE} \sim \int \langle \Phi(0)\Phi(\tilde{\mathrm{r}}) \rangle \exp(\mathrm{i}\tilde{\mathrm{q}} \cdot \tilde{\mathrm{r}})\, \mathrm{d}^{\mathrm{d}}\mathrm{r}, \tag{18}$$

where, $\langle \Phi(0)\Phi(\vec{r}) \rangle$ is the order parameter correlation function and d the dimensionality of the system. The rationale behind the droplet model is that the NDE signal results from the scattered intensity caused by the effective dipole-dipole correlations in the system, the same way light scattering intensity results from density-density correlations.

As shown by de Gennes and Prost[54], the droplet model leads to the experimentally observed scaling for NDE in the vicinity of a liquid-liquid critical point in three dimensions, namely, $\text{NDE} \sim \xi^{\mathrm{d}-1-\eta}$, with $\xi = \xi_o t^{-\nu}$, and $t = |T - T_c|/T_c$. The theoretically predicted NDE scaling for this system (Ising symmetry, d=3) is therefore,

$$\begin{cases} t^{-(2-\eta)\nu} & d = 3, \text{Ising}; \qquad \text{e.g., liquid-liquid} \\ t^{-1.25} & \nu = 0.64, \eta = 0.041; \qquad \text{3-d Ising model} \\ t^{-1.28} & \nu = 0.64, \eta = 0; \qquad \text{Ornstein-Zernikie} \\ t^{-1} & \nu = 0.5, \eta = 0; \qquad \text{Mean field theory} \\ t^{-1} & \text{dipolar fluids}; \qquad \text{experiment}[45]. \end{cases} \tag{19}$$

Encouraged by the agreement of the phenomenological NDE scaling laws with experiment for systems with Ising symmetry, we derive the analogous NDE scaling laws near the liquid-hexatic, and hexatic-crystal phase boundaries. Our analysis was greatly facilitated because Halperin and Nelson[2] and Young[2] have worked out the scaling of the relevant order parameter correlations to be used in equations 15 and 17. The order parameter correlations above the transition temperatures for the liquid-hexatic and hexatic-crystal transitions have the form, $G_{T,6}(r) \sim \exp(-r/\xi_+)$, where the subscripts $T, 6$ correspond to translational and orientational correlation functions, and + refers to the correlation function above the transition temperature, i.e., $t > 0$. Above the hexatic-liquid phase transition temperature, $\xi_+ = A\exp(B/|t|^\nu)$, with $\nu = 0.5$ based on a renormalization group analysis. Similarly, the translational order parameter correlation length is given by $\xi_+ = A\exp(B/|t|^\nu)$, with $\nu = 0.37$ for a smooth substrate, above the crystal-hexatic phase boundary. The phenomenological NDE scaling directly follows from using equation 17 (note that $\eta = 0, d = 2$),

$$1/\mathrm{NDE} = \mathrm{A}\exp(-\mathrm{B}/|\mathrm{T} - \mathrm{T_c}|^\nu) \tag{20}$$

with $\nu = 0.5$ for the liquid-hexatic (high temperature) transition and $\nu = 0.37$ for the hexatic-crystal (low temperature) transition.

The NDE scaling with temperature for confined aniline is re-plotted in figure 8 along with the NDE scaling law (equation 20). The results show the consistency of the NDE signals with KTHNY scaling laws for the liquid-hexatic and hexatic-crystal transitions. The estimates for the exponent ν for liquid-hexatic and hexatic-crystal transitions based on the experimental measurements is currently not possible owing to the nature of the ACF sample; true divergence is not observed in our measurements as the length of the in-plane correlations in the fluid are curtailed by the finite size of the graphitic microcrystals in ACF. Therefore, NDE signals close to the transition temperatures for an infinite system are not accessible in our experiments. Instead, the NDE signals in our experiment correspond to a finite system size of 5 nm, the average size of the graphitic microcrystal (in the xy plane) in our ACF-A10 sample.

Fig. 8

VII. DISCUSSION

Our computer simulations for a bilayer of adsorbed fluid in a slit-pore with smooth walls has established the existence of two-stage melting in the thermodynamic limit via system size scaling analysis. Based on the calculations of the Ginzburg parameter we establish that for system sizes smaller than 60 molecular diameters, fluctuations are too large to uphold the finite size simulation results. Based on the Lee-Kosterlitz scaling of the free energy surface, we establish that the transitions are first order in the thermodynamic limit. Similar results for a monolayer established that the transitions were continuous. Our experimental results rely on indirect evidence based on phase transitions (structural measurements are considered direct evidence). Nevertheless, the quantitative agreement between the simulations and DSC, DRS, and NDE measurements, make a strong case for the existence of KTHNY melting and therefore a hexatic phase in the confined system. This interpretation, if correct, shows that the hexatic phase is stable over a wide temperature range, 55 K for CCl_4 and 26 K for aniline. This large range of state conditions over which the hexatic phase is stable may be unique to confined fluids in porous media.

Effect of the Six-Fold Potential. The main difference between the simulation results and the experimental results reported in this paper is that the former corresponds to a smooth substrate, while the latter corresponds to a substrate with 6-fold symmetric potential. On a theoretical basis, the effects of the six-fold symmetry of the pore potential and that of the finite size of the graphitic microcrystals combined might be expected to nullify the liquid-hexatic phase transition and cause a rounding of divergences associated with the hexatic-crystal transitions. The latter is observed in the NDE measurements (the NDE signals do not diverge), while the former manifests itself as a remnant KTHNY behavior, presumably due to a weak six-fold substrate potential. It is worth pointing out that the LJ diameters of CCl_4 and aniline (0.5-0.6 nm) are much larger than the C-C bond length in graphite (0.14 nm), so that the fluid molecules only feel a mild corrugation in the fluid-wall

potential in passing along the surface. This feature contrasts with the situation for earlier experiments concerning Xe, Ar, and Kr on graphite substrates, where the LJ diameters for the fluid are much smaller and comparable to the C-C spacing in graphite. There is evidence of an intrinsic hexatic phase even for the case of Xe in graphite[15,16]; therefore, for substrate molecules larger than Xe, we expect the crystal to melt into a hexatic phase with intrinsic stiffness with respect to bond-orientational fluctuations. While we note the quantitative agreement in transition temperatures between simulations and experiments and have described the respective domains of validity, the question of whether an intrinsic hexatic phase is observed in a realistic simulation with six-fold symmetric substrate potential remains to be answered. Simulations are currently in progress to address this question. On the experimental side, the challenge is to synthesize a porous sample with uniform pores with large microcrystal sizes to examine the scaling for several decades in $|T - T_c|/T_c$ on a log scale, and to obtain direct structural evidence of the hexatic phase via scattering experiments.

Effect of Multi-Layers on KTHNY Melting. The scaling of the order-parameter correlation functions in the simulations (figure 2) are consistent with the KTHNY behavior, implying that it is the vortex excitations that govern the equilibrium behavior in the quasi-two-dimensional systems and that the melting transition is defect-mediated. Moreover, for a quasi-two-dimensional monolayer, the Kosterlitz-Thouless transitions are continuous[37], while for quasi-two-dimensional bilayers the Kosterlitz-Thouless transitions become first-order (figure 3). We ascribe this deviation from 2-d behavior to the interactions between the defect configurations in different layers, based on the following scaling arguments.

On heuristic grounds[3], the free energy of exciting a vortex pair of opposite winding numbers relative to the ordered phase in the xy model in 2-d is given by $\Delta F = (\pi J - 2k_B T)\log(L)$, J being the interaction energy of two neighboring spins with the same alignment and L being the distance between the vortex cores. This is the essence of the Kosterlitz-Thouless (KT) transition. If we consider two planes of xy mod-

els interacting with each other, and the vortices in one layer are perfectly in alignment with those in the second layer, the free energy relative to the ordered phase is given by $\Delta F^{(\mathrm{KT})} = (2\pi J - 2k_B T)\log(L)$, which is qualitatively the same as the KT behavior. This configuration, however, corresponds to a reduced entropy situation because the number of different ways of placing the aligned vortex pairs is the same as the single layer case. A second higher entropy scenario exists, where a vortex in one layer is aligned with a vortex of the opposite winding number in the other layer, with the cores displaced by distance A. Such a situation corresponds to a free energy (see Appendix):

Appendix

$$\Delta F = \Delta F^{\mathrm{KT}} + (\pi - 1)J'L^2 + J'AL\ln L - k_B T \ln(1 + \pi A^2) \tag{21}$$

where J is the interaction of nearest neighbors of spins with the same alignment, L is the in-plane distance between vortex cores, $\Delta F^{(\mathrm{KT})} = (2\pi J - 2k_B T)\log(L)$ is the Kosterlitz-Thouless free energy[3], J' is the nearest-neighbor interaction between layers and in general can be different from J, and A is the "offset-distance" between vortices as defined above. Treating L as the order parameter, the free energy profile is obtained by the locus of points that minimize ΔF, the variational parameter being A. The locus of points minimizing ΔF is qualitatively different from that for the true KT behavior, given by $\Delta F^{(\mathrm{KT})}$ (figure 9) . In particular, at small separations of the vortices, the bound state actually exists as a metastable state for $T > T_c$, a clear signature of a first-order phase transition. Figure 9 depicts the free energy profile for the monolayer case and bilayer case at a temperature $k_B T = 1.5$, assuming $2\pi J = 1$ and $(\pi - 1)J' = 0.2$ (where J, J' are in units of $k_B T$). The plot marked by the solid line represents $\Delta F^{(\mathrm{KT})}$, the true KT scenario, at a temperature, T, greater than the transition temperature, T_c, for which the lowest free energy state corresponds to $L = \infty$, i.e., the vortices are unbound. Moreover, the bound state ($L = 1$) is unstable and remains so, as long as $T > T_c$, and therefore the transition is continuous (second-order). The set of dotted lines are plotted according to equation (21) for different values of the offset distance A. It is immediately clear that the locus of points minimizing ΔF is qualitatively different from the KT plot (equation for $\Delta F^{(\mathrm{KT})}$). In particular, at small separations of the vortices,

Fig. 9

the bound state actually exists as a metastable state for $T > T_c$, a clear sign of a first-order phase transition. In other words, the vortex excitations that lead to equation A-7 (see Appendix) imply a pathway for nucleation of the ordered phase, i.e., by the annihilation of vortices $\vec{U}^+$ and $\vec{U}^-$ across layers. This is possible only if hopping of particles between layers are allowed, such as in our confined fluid system.

The simulations and above arguments pertain to smooth pore walls. Therefore, the effect of the six-fold substrate potential was ignored while taking into account the strong potential due to the porous matrix. To our knowledge, this is the first report of the effect of multi-layers on KTHNY behavior.

Effect of Strength of the Pore Potential. It was remarked earlier, based on the evidence from simulations and experiments, that the hexatic phase was stable over a large temperature range for CCl_4 and aniline. The ratio of the strength of the fluid-wall interaction to the fluid-fluid interaction, α (equation 3), has a significant effect on the melting phase diagram[33] (see figure 10); in particular, the larger the value of α, the larger the temperature range over which the hexatic phase is stable. Therefore, fluids with purely dispersive interactions (e.g., CCl_4, methane, benzene etc.) confined in ACF, with large values of α show a large temperature range of stability for the hexatic phase. For strongly dipolar fluids, α is smaller, the temperature range of stability of the hexatic phase decreases[33], and may vanish for sufficiently small α.

Fig. 10

We acknowledge funding from NSF under grant number CTS-0211792 and from KBN under grant number 2 PO3B 01424. The experiments were performed in Adam Mickiewicz University, Poznan, Poland. The supercomputing time was provided by the San Diego Supercomputing Center under a NRAC grant (number MCA93S011P). International cooperation was supported by a NATO Collaborative Linkage grant (no. 978802).

REFERENCES

[1] N.D. Mermin, and H. Wagner, Phys. Rev. Lett. **17**, 1133 (1966).

[2] B.I Halperin, and D.R. Nelson, Phys. Rev. Lett. **41**, 121 (1978); D.R. Nelson and B.I. Halperin, Phys. Rev. B **19**, 2457 (1979). A.P. Young, Phys. Rev. B **19**, 1855 (1979).

[3] J.M. Kosterlitz, and D.J. Thouless, J. Phys. C **5**, L124 (1972); J.M. Kosterlitz, and D.J. Thouless, J. Phys. C **6**, 1181 (1973).

[4] S. T. Chui, Phys. Rev. Lett. **48**, 933 (1982); S. T. Chui, Phys. Rev. B. **28**, 178 (1983).

[5] K.J. Strandburg, Rev. Mod. Phys. **60**, 161 (1988); K.J. Strandburg (editor), Bond Orientational Order in Condensed Matter Systems, Springer-Verlag:New York (1992).

[6] R. Pindak, D. E. Moncton, S. C. Davey, and J. W. Goodby, Phys. Rev. Lett. **46**, 1135 (1981); J. D. Brock, R. J. Birgeneau, J. D. Lister, and A. Aharony, Physics Today, July, 52 (1989); J. D. Brock, A. Aharony, R. J. Birgeneau, K. W. Evans-Lutterody, J. D. Litster, P. M. Horn, G. B. Stephenson, and A. R. Tajbakhsh, Phys. Rev. Lett. **57**, 98 (1986); C.Y. Chao, C.F. Chou, J.T. Ho, S.W. Hui, A. Jin, and C.C. Huang, Phys. Rev. Lett. **77**, 2750 (1996); C. F. Chou, A. J. Jin, S. W. Huang and J. T. Ho, Science **280**, 1424 (1998).

[7] I . M. Jiang, T. Stoebe, and C. C. Huang, Phys. Rev. Lett. **76**, 2910 (1996); D. L. Lin, J. T. Ou, L. P. Shi, X. R. Wang, A. J. Jin, Europhys. Lett. **50**, 615 (2000).

[8] C. H. Murray, D. H. Van Winkle, Phys. Rev. Lett. **58**, 1200 (1988).

[9] A.H. Marcus and S.A. Rice, Phys. Rev. E. **55**, 637 (1997).

[10] P. Karnchanaphanurach, B. Lin and S.A. Rice, Phys. Rev. E. **61**, 4036 (2000).

[11] K. Zahn, R. Lenke, G. Maret, Phys. Rev. Lett. **82**, 2721 (1999).

[12] P. A. Heiney, P. W. Stephens, R. J. Birgeneau, P. M. Horn, and D. E. Moncton, Phys. Rev. B. **28**, 6416 (1983).

[13] E. D. Specht, M. Sutton, R. J. Birgeneau, D. E. Moncton, and P. M. Horn, Phys. Rev. B. **30**, 1589 (1984).

[14] J. P. McTague, J. Als-Nielsen, J. Bohr, and M. Nielsen, Phys. Rev. B **25**, 7765 (1982).

[15] S. E. Nagler, P. M. Horn, T. F. Rosenbaum, R. J. Birgeneau, M. Sutton, S. G. J. Mochrie, D. E. Moncton, and R. Clarke, Phys. Rev. B **32**, 7373 (1983).

[16] N. G. Greiser, A. Held, R. Frahm, R. L. Greeme, P. M. Horn, M. Suter, Phys. Rev. Lett. **59**, 1625 (1987).

[17] F. C. Motteler, Ph.D. thesis: University of Washington (1985).

[18] H. K. Kim, Q. M. Zhang, and M. H. W. Chan, Phys. Rev. Lett. **56**, 1579 (1986).

[19] Q. M. Zhang, Feng, H. K. Kim, M. H. W. Chan, Phys. Rev. Lett. **57**, 1456 (1986); Q. M. Zhang, H. K. Kim, M. H. W. Chan, Phys. Rev. B **33**, 5149 (1986).

[20] C. Undink, J. van der Elsken, Phys. Rev. B. **35**, 279 (1987).

[21] M. A. Stan, A. J. Dham, Phys. Rev. B. **40**, 8995 (1989).

[22] H. Weber, D. Marx, K. Binder, Phys. Rev. B. **51**, 14636 (1995).

[23] K. Bagchi, H. C. Andersen, W. Swope, Phys. Rev. Lett. **76**, 255 (1996).

[24] A. Jaster, Phys. Rev. E. **59**, 2594 (1999).

[25] P. Bladon and D. Frenkel, Phys. Rev. Lett. **74**, 2519 (1995).

[26] R. Zangi and S. A. Rice, Phys. Rev. E. **58**, 7529 (1998).

[27] S. Sengupta, P. Nielaba, K. Binder, Phys. Rev. E. **61**, 6294 (2000).

[28] F. F. Abraham, Phys. Rev. Lett. **44**, 463 (1980); F. F. Abraham, Phys. Rep. **80**, 339 (1981); F. F. Abraham, Phys. Rev. B **23**, 6145 (1981); F. F. Abraham, Phys. Rev. Lett. **50**, 978 (1983); F. F. Abraham, Phys. Rev. B **29**, 2606 (1984).

[29] M. W. Roth, Phys. Rev. B. **57**, 12520 (1998).

[30] A. Alavi, Phys. Rev. Lett. **64**, 2289 (1990).

[31] L. D. Gelb, K. E. Gubbins, R. Radhakrishnan, M. Sliwinska-Bartkowiak, Rep. Prog. Phys. **62**, 1573 (1999).

[32] W. A. Steele, Surf. Sci. **36**, 317 (1973).

[33] R. Radhakrishnan, K. E. Gubbins, and M. Sliwinska-Bartkowiak, J. Chem. Phys. **116**, 1147 (2002).

[34] J. S. Van Duijneveldt, D. Frenkel, J. Chem. Phys. **96**, 4655 (1992).

[35] R. M. Lynden-Bell, J. S. Van Duijneveldt, D. Frenkel, Mol. Phys **80**, 801 (1993).

[36] R. Radhakrishnan and K. E. Gubbins, Mol. Phys. **96**, 1249 (1999).

[37] R. Radhakrishnan, K. E. Gubbins, and M. Sliwinska-Bartkowiak, Phys. Rev. Lett. **89**, 076101 (2002).

[38] L. D. Landau, E. M. Lifshitz, Statistical Physics., Part 2, Ch. 5, 3rd edn. London:Pergamon Press, (1980).

[39] N. D. Mermin, Phys. Rev. **176**, 250 (1968).

[40] G. M. Torrie, J. P. Valleau, Chem. Phys. Lett. **28**, 578 (1974).

[41] A. Watanabe, K. Kaneko, T. Iiyama, R. Radhakrishnan, and K. E. Gubbins, J. Phys. Chem. **103**, 7061 (1999).

[42] K. Oshida, M. Endo, Private Communication (1998).

[43] P. Debye, *Polar Molecules* (Chemical Catalog Co., New York, 1929).

[44] M. Sliwinska-Bartkowiak, J. Gras, R. Sikorski, R. Radhakrishnan, L. D. Gelb and K. E. Gubbins, Langmuir **15**, 6060 (1999).

[45] A. Chelkowski, Dielectric Physics, Elsevier, North-Holland Inc.: New York, p. 292 (1980).

[46] M. Sliwinska-Bartkowiak, B. Szurkowski, and T. Hilczer, Chem. Phys. Lett. **94**, 609 (1983).

[47] V. Privman (Ed.), Finite size scaling and numerical simulation in statistical systems, World Scientific:New York, p. 173 (1990).

[48] K. K. Mon and K. Binder, J. Chem. Phys. **96**, 6989 (1992).

[49] P. M. Chaikin, and T. C. Lubensky, Principles of Condensed Matter Physics, Cambridge University Press:Cambridge, p. 39 (1995).

[50] H. E. Stanley, Introduction to phase transitions and critical phenomena, Ch. 3, Ch. 4, Ch. 7, Oxford University press: New York (1971).

[51] J. Lee and J.M. Kosterlitz, Phys. Rev. Lett. **65**, 137 (1990).

[52] M. Sliwinska-Bartkowiak, R. Radhakrishnan,K. E. Gubbins, Mol. Sim. **27**, 323 (2001).

[53] D. W. Oxtoby, H. Metiu, Phys. Rev. Lett. **36**, 1092 (1976); D. W. Oxtoby, Phys. Rev. A **15**, 1251 (1977).

[54] P. G. De Gennes, J. Prost, Molecular theory of liquid crystals, Oxford University Press:Oxford, p80 (1995),

[55] M. Sliwinska-bartkowiak, G. Dudziak, R. Sikorski, R. Gras, K. E. Gubbins, and R. Radhakrishnan, Phys. Chem. Chem. Phys., **3**, 1179 (2001).

[56] R. Radhakrishnan, K. Gubbins, and M. Sliwinska-Bartkowiak, J. Chem. Phys. **112**, 11048 (2000).

[57] A. Watanabe and K. Kaneko, Chem. Phys. Lett., **305**, 71 (1999).

APPENDIX

We give here the derivation of equation 21 for a bilayer of the xy model of spins on a lattice. We consider two planes of xy models interacting with each other; vortices with opposite winding numbers in one layer are perfectly in alignment with those in the second layer (i.e, the vortex cores span two layers). The free energy relative to the ordered phase is given by[3]:

$$\Delta F^{(\mathrm{KT})} = (2\pi J - 2k_B T)\log(L) \tag{A-1}$$

which is qualitatively the same as the KT behavior (solid line in figure 9). This configuration, however, corresponds to a reduced entropy situation because the number of different ways of placing the aligned vortex pairs is the same as the single layer case. A second, higher entropy scenario exists, where a vortex in one layer is aligned with a vortex of the opposite winding number in the other layer, with the cores displaced by distance A.

Vortices of positive and negative winding numbers whose cores are displaced by length A are represented as vector fields $\vec{U}^+$ and $\vec{U}^-$, given by:

$$\vec{U}^+ \;=\; (x-A)\hat{e}_x \;-\; y\hat{e}_y \tag{A-2}$$

$$\vec{U}^- \;=\; -y\hat{e}_x \;+\; (x-A)\hat{e}_y \tag{A-3}$$

where e_x, e_y are unit vectors in the x and y directions. The interaction energy E relative to the ordered phase, for the given spin fields $\vec{U}^+$ and $\vec{U}^-$ in each layer, is given by:

$$E \;=\; J' \int_0^L \int_0^L \vec{U}^+ \cdot \vec{U}^- \, dx\, dy \;+ \pi J' L^2 \tag{A-4}$$

$$\;=\; (\pi - 1)J'L^2 \;+\; J'AL\ln L \tag{A-5}$$

and the excess entropy associated with placing the cores with an offset distance A is given by $S = k_B \ln(1+\pi A^2)$. The free energy relative to the ordered state is given by:

$$F \;=\; 2\pi J \ln L \;-\; 2k_B T \ln L \;+\; (\pi-1)J'L^2 \;+\; J'AL\ln L - k_B T \ln(1+\pi A^2) \tag{A-6}$$

$$\;=\; \Delta F^{\mathrm{KT}} \;+\; (\pi-1)J'L^2 \;+\; J'AL\ln L - k_B T \ln(1+\pi A^2) \tag{A-7}$$

FIGURES

FIG. 1. Orientational correlation functions for the confined bilayer of adsorbate ($H = 1.41$ nm): liquid (360 K), hexatic (335 K), and crystal (290 K) phases.

FIG. 2. Scaling behavior of orientational correlation functions. The solid line corresponds to zero slope, the dashed line corresponds to a slope of $-1/4$ and the dotted line corresponds to a slope of -2.

FIG. 3. (a) Landau free energy functions for two different system sizes $60\sigma_{\rm ff}$ and $180\sigma_{\rm ff}$ for a pore width of $H = 1.41$ nm at the hexatic-crystal transition. The temperature was $T = 293$ K for the $60\sigma_{\rm ff}$ system, and $T = 290$ K for the $180\sigma_{\rm ff}$ system. (b) Corresponding results for $H = 0.91$ nm system at the liquid-hexatic transition, for the $60\sigma_{ff}$ system ($T = 390$ K) and $180\sigma_{ff}$ ($T = 387$ K).

FIG. 4. The grand free energy per mole for liquid, hexatic and crystal phases ($H = 1.41$ nm); the cross-over points correspond to phase transitions and give the transition temperatures (see Table II).

FIG. 5. DSC scan for CCl_4 and aniline confined in activated carbon fiber ACF A-10 at a temperature scanning rate of 0.1 K/min. The peaks are interpreted as the liquid-hexatic (high T) and hexatic-crystal (low T) transitions. The approximate transition temperature is located at the tail of each peak in the low temperature side (see Figure 9.4.3 on page 550 of Chaikin and Lubensky[49]).

FIG. 6. DRS temperature scan (the sample was equilibrated at each temperature) for aniline confined in ACF-A10, as a function of temperature indicating phase transitions (dashed lines), (a) capacitance; (b) molecular orientational relaxation time (τ). The disappearance of the relaxation branch due to conductance of the sample is believed to correspond to the liquid-hexatic transition, and the change in the relaxation time of the confined fluid is interpreted as the occurrence of the hexatic-crystal phase transition[52]. The relaxation branch corresponding to the Maxwell-Wagner effect occurs as a result of signal dispersion due to the suspended ACF particles in bulk aniline[52].

FIG. 7. NDE for (a) CCl_4, and (b) aniline, confined in activated carbon fiber ACF A-10. The peaks correspond to the liquid-hexatic (L/H) and hexatic-crystal (H/C) transitions. Lines are drawn through the points as guide to the eye.

FIG. 8. NDE scaling for aniline confined in activated carbon fiber ACF A-10. The filled circles correspond to liquid above the L/H phase transition, and the filled squares correspond to the hexatic above the H/C phase transition. The solid lines represent a fit to the scaling law with the theoretically predicted exponents (see legend). For the liquid (filled circles) $A = \exp(34.52)$, $B = 6.48$, $\nu = 0.5$, $T_c = 42°$C; for the hexatic (filled squares) $A = \exp(32.46)$, $B = 0.338$, $\nu = 0.37$, $T_c = 27°$C.

FIG. 9. Free energy scaling for a set of interacting vortex pairs in a bilayer according to the equation for $\Delta F^{(\mathrm{KT})}$ and equation 21. The distances L and A are in dimensionless units (scaled by the lattice length) and the free energy is in units of $k_B T$.

FIG. 10. Global phase diagram of a fluid in a slit pore of width $H = 3\sigma_{\mathrm{ff}}$ from simulations and free energy calculations[33,37] (open symbols) and experiment (filled symbols)[33,37,55,56,52,41,57]. Three different phases are observed: liquid (L), hexatic (H), and crystalline (C). The dashed line represents an extrapolation of the phase boundaries based on MC simulations without free energy calculations. The simulations are for a LJ fluid in slit-pore with different values of α. The experiments are for various adsorbates confined within activated carbon fibers (ACF, mean pore width 1.4 nm): H_2O[55] ($\alpha = 0.51$), $C_6H_5NO_2$[56] ($\alpha = 1.22$), $C_6H_5NH_2$[52] ($\alpha = 1.75$), CH_3OH[55] ($\alpha = 1.82$), CCl_4[41,37] ($\alpha = 1.92$), C_6H_6[57] ($\alpha = 2.18$).

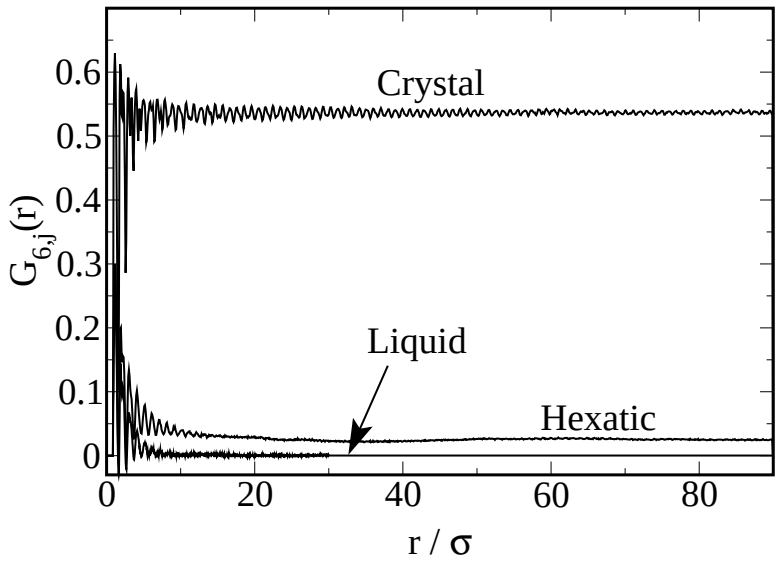
Crystal
Liquid
Hexatic
$G_{6,j}(r)$
r / σ
0
0.1
0.2
0.3
0.4
0.5
0.6
0
20
40
60
80

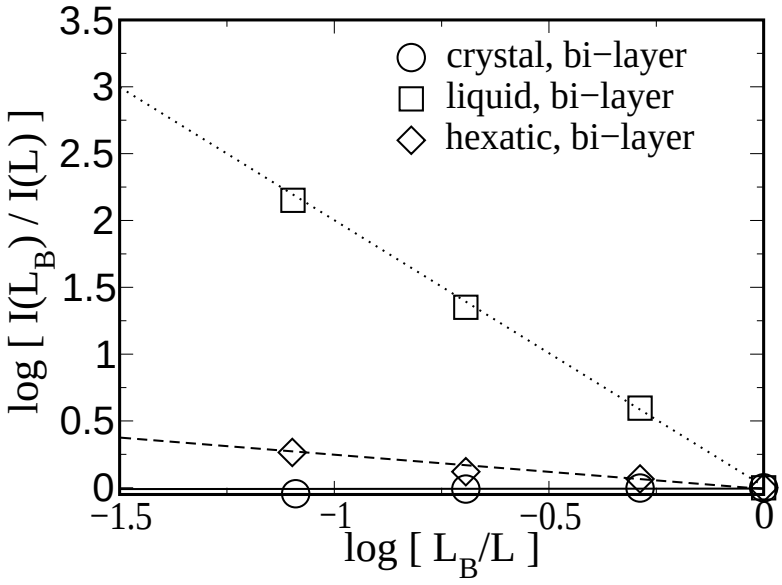
crystal, bi−layer
liquid, bi−layer
hexatic, bi−layer
log [I(L_B) / I(L)]
log [L_B/L]
3.5
3
2.5
2
1.5
1
0.5
0
−1.5
−1
−0.5
0

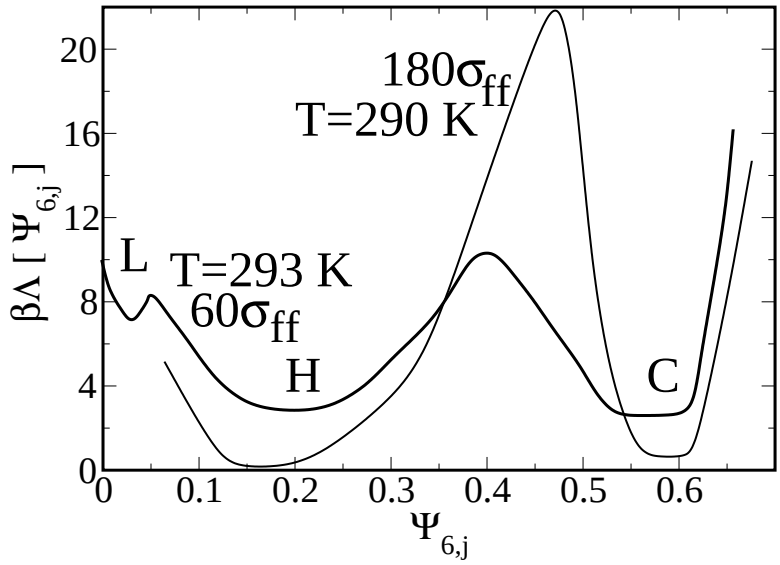
180σff
T=290 K
L
T=293 K
60σff
H
C
βΛ [Ψ6,j]
Ψ6,j
0
4
8
12
16
20
0
0.1
0.2
0.3
0.4
0.5
0.6

(a)

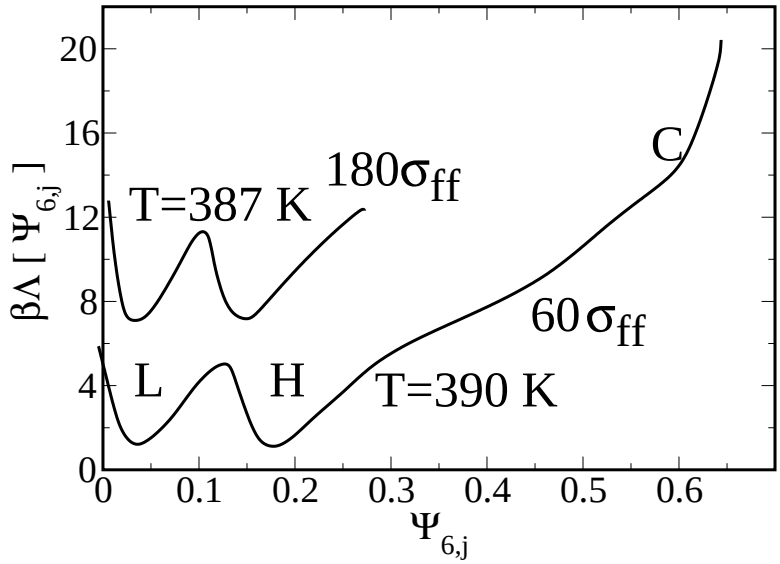
C
180σff
T=387 K
60 σff
L
H
T=390 K
βΛ [Ψ6,j]
Ψ6,j
0
4
8
12
16
20
0
0.1
0.2
0.3
0.4
0.5
0.6

(b)

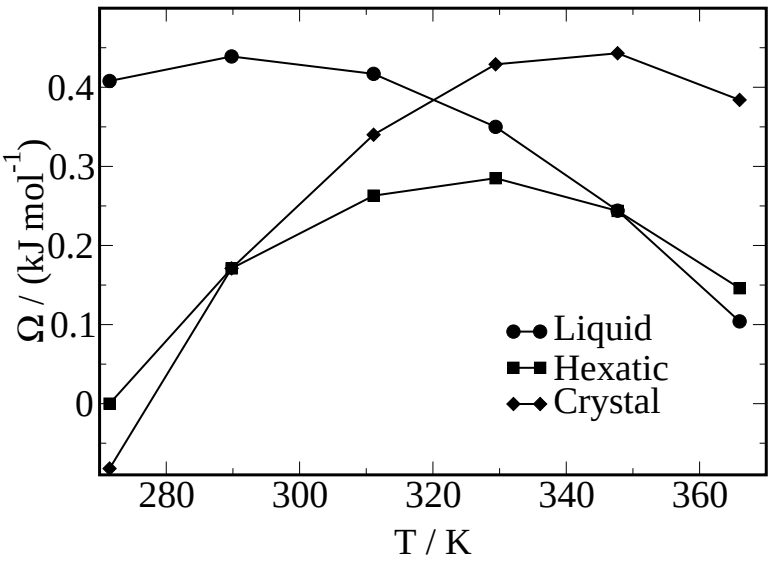
0.4
0.3
0.2
0.1
0
Ω / (kJ mol-1)
280
300
320
340
360
T / K
Liquid
Hexatic
Crystal

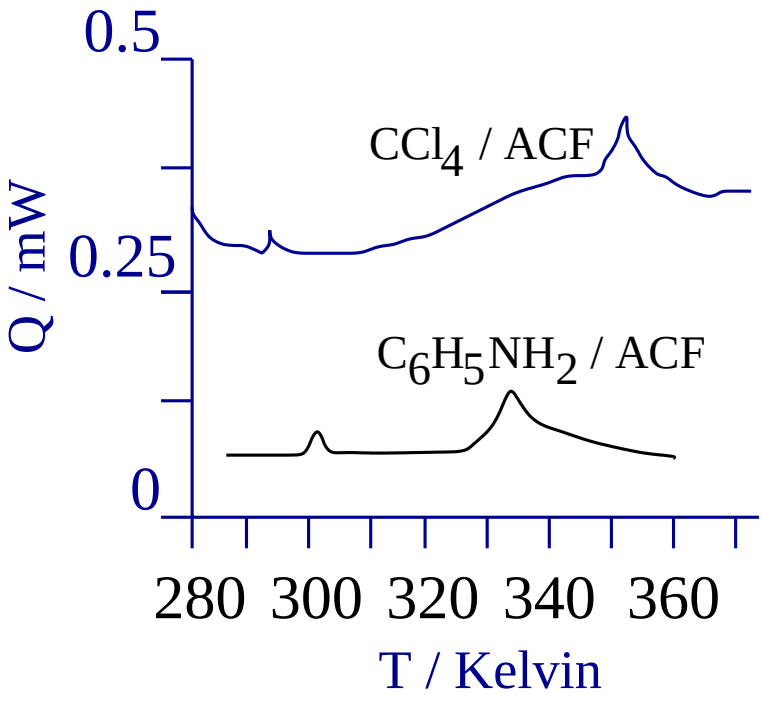
0.5
0.25
0
Q / mW
CCl_4 / ACF
$C_6H_5NH_2$ / ACF
280 300 320 340 360
T / Kelvin

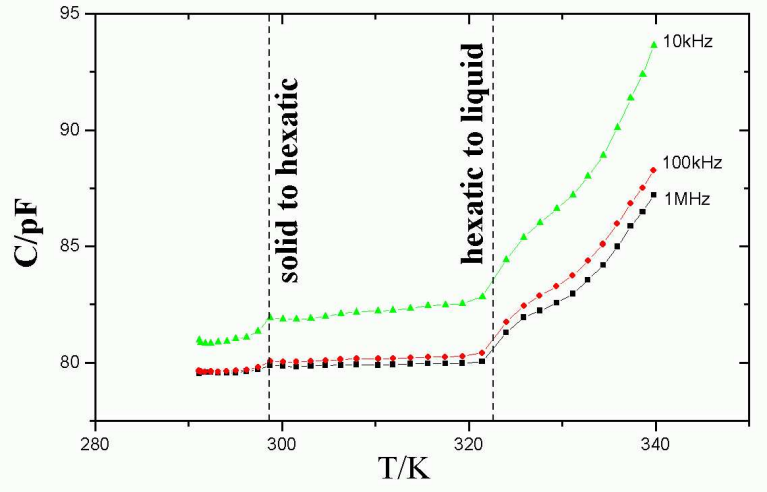
C/pF
T/K
solid to hexatic
hexatic to liquid
10kHz
100kHz
1MHz

(a)

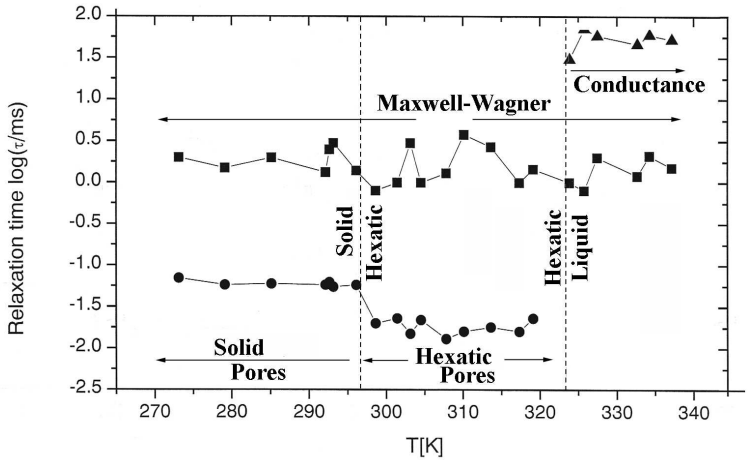
Relaxation time log(τ/ms)
T[K]
Maxwell-Wagner
Conductance
Solid
Hexatic
Hexatic
Liquid
Solid
Pores
Hexatic
Pores

(b)

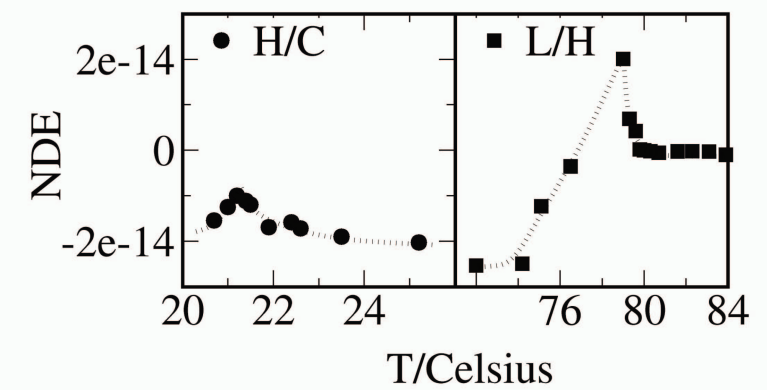
H/C
L/H
2e-14
0
-2e-14
NDE
20
22
24
76
80
84
T/Celsius

(a)

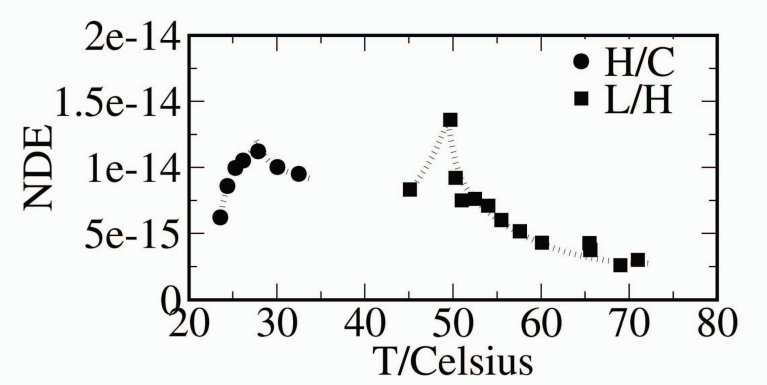
2e-14
1.5e-14
1e-14
5e-15
0
NDE
H/C
L/H
20
30
40
50
60
70
80
T/Celsius

(b)

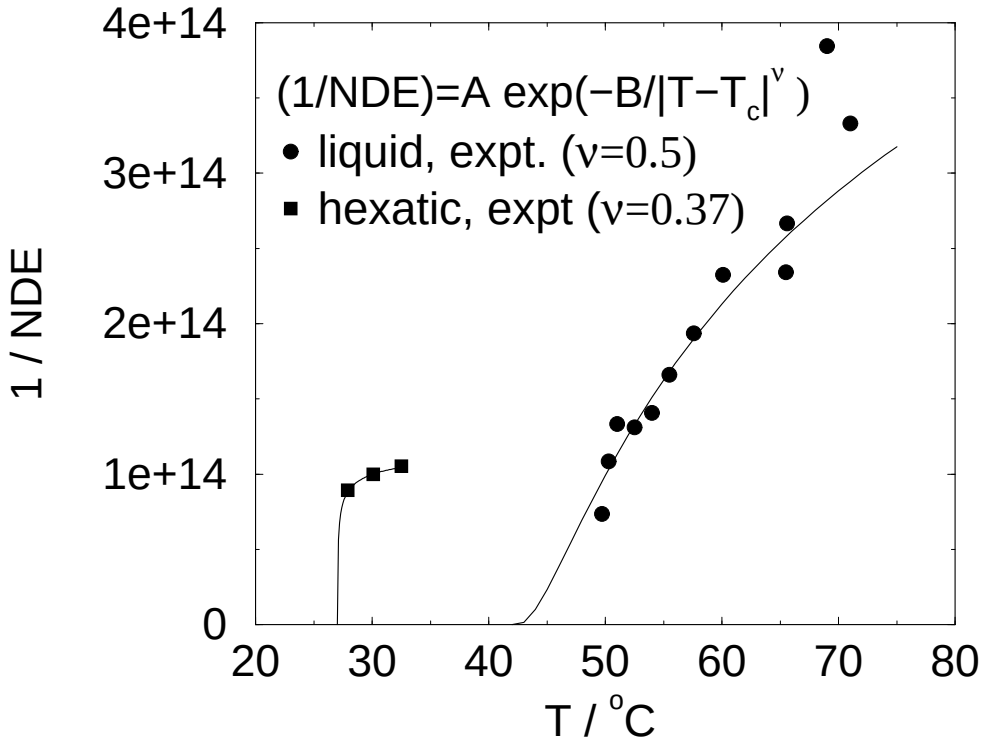
4e+14
3e+14
2e+14
1e+14
0
1 / NDE
20
30
40
50
60
70
80
T / °C
(1/NDE)=A exp(−B/|T−T_c|^ν)
liquid, expt. (ν=0.5)
hexatic, expt (ν=0.37)

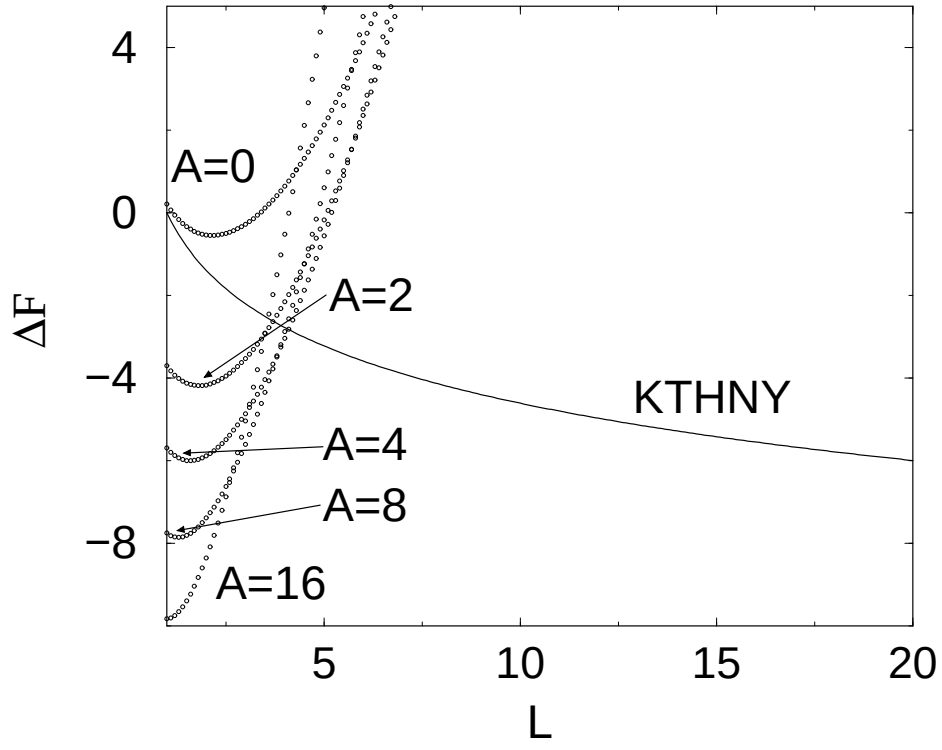
4
0
−4
−8
ΔF
A=0
A=2
A=4
A=8
A=16
KTHNY
5
10
15
20
L

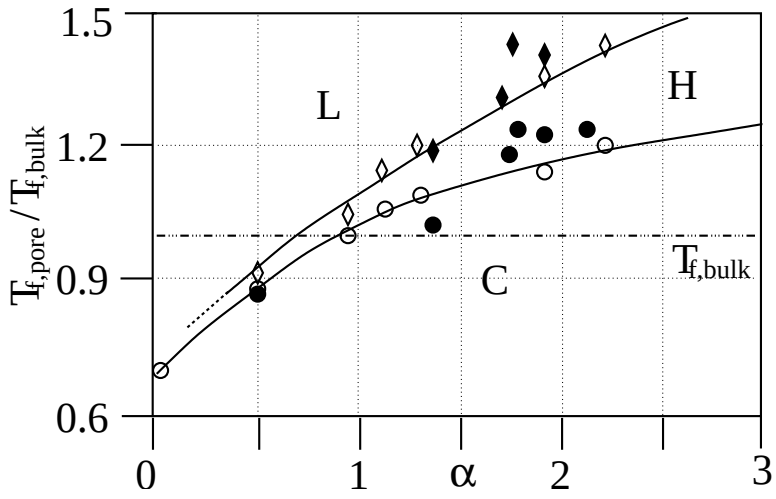
1.5
1.2
0.9
0.6
0
1
α
2
3
L
H
C
$T_{f,bulk}$
$T_{f,pore} / T_{f,bulk}$

Table I: Ginzburg parameter for different L and T.

T/K	$10\sigma_{\rm ff}$	$40\sigma_{\rm ff}$	$60\sigma_{\rm ff}$	$180\sigma_{\rm ff}$
340	8.98	1.95	0.117	0.038
330	6.4	1.7	0.102	0.029
320	4.29	1.17	0.098	0.019
310	3.11	0.97	0.16	0.0189
300	3	0.937	0.176	0.0189

Table II. Transition temperatures from simulation and experiment for CCl_4 and aniline in ACF-10.

Fluid	Low T_c/K (H/C)		High T_c/K (L/H)	
	Simulation	Expt.	Simulation	Expt.
CCl_4	290	298[a], 295[b,c]	348 K	348[a], 353[b], 352[c]
Aniline	–	301[a], 298[b], 300[c]	–	325[a], 324[b], 315[c]

[a]DSC, [b]DRS, [c]NDE